Finite-Amplitude Perturbation Thresholds for Subcritical Transition in Taylor-Couette Flow

by

Katherine LaChasse

Submitted in Partial Fulfillment of the
Requirements for the Degree

Bachelor of Arts

Supervised by
Daniel Borrero-Echeverry

Department of Physics

Willamette University, College of Liberal Arts
Salem, Oregon

2019

Presentations and Publications

- "Finite-Amplitude Perturbation Thresholds for Subcritical Transition in Taylor-Couette Flow". Oral Presentation, Annual Senior Symposium (May 2019)

- "Finite-Amplitude Perturbation Thresholds for Subcritical Transition in Taylor-Couette Flow". Poster, Annual Senior Symposium (May 2019)

- "Finite-Amplitude Perturbation Thresholds for Subcritical Transition in Taylor-Couette Flow". Oral Presentation, Senior Research Seminar II: Final Presentation (April 2019)

- "Effects of Axial Aspect Ratio and Perturbation Location on the Subcritical Transition to Turbulence in Taylor-Couette Flow". Oral Presentation, Senior Research Seminar I: Status Report Presentation (December 2018)

- "Using Machine Vision to Study the Subcritical Transition to Turbulence in Taylor-Couette Flow". Poster, Murdock College Science Research Conference (November 2018)

- "Using Machine Vision to Study the Subcritical Transition to Turbulence in Taylor-Couette Flow". Oral Presentation, Science Collaborative Research Program Symposium (September 2018)

Acknowledgments

I would like to thank the Mary Stuart Rogers Foundation and Willamette University's Science Collaborative Research Program for providing the opportunity and funding to begin my research early.

I would also like to thank the entire Physics Department at Willamette for creating such a wonderful environment to learn and grow. I could not ask for a better advisor than Dr. Rick Watkins for my undergraduate years. Thank you for shaping me into the physicist I am today. Thank you Dr. Jed Rembold for greatly assisting me with my Python code, my data table, and for letting me shoot the breeze in your office for hours. Caspar Croft, Hannah Rarick, and the rest of the Splash Zone's help has been integral in the completion of this thesis.

Finally, I would like to thank my thesis advisor, Dr. Daniel Borrero, for the constant support he has shown me during the course of this thesis, both in and out of the lab. Your encouragement and guidance made it possible to continue working in spite of all the leaks, cracks, and countless other obstacles.

Abstract

General Abstract: Turbulence, a highly complex flow regime, is the preferred state for most fluid flows and essential in many applications. However, the transition from smooth, laminar flow to turbulence is not well understood. To better understand this phenomenon we analyzed the transition in a Taylor-Couette system, a fluid flow found in the gap between two rotating cylinders. While holding the inner cylinder stationary and rotating the outer cylinder at different angular velocities, we can change the Reynolds number (Re), a dimensionless quantity describing the state of the flow. We introduced injections of fluid with a variety of flow rates to rotating, laminar flow to determine what combinations of Re and perturbation amplitude would induce turbulence. From this, we analyzed the relationship between the smallest perturbation that would transition for a given Re, and found that it scales like $Re^{-0.905}$. Our value of -0.905 ± 0.1 is in agreement with the upper bounds of the theoretical predictions, which suggest that it should be between between -4 and -1.

Technical Abstract: Turbulence, a flow regime characterized by a high degree of spatiotemporal complexity and irregular fluctuations, is not well understood despite its importance and prevalence. Especially important is that there is no general theory that predicts when smooth, laminar flow will become turbulent. In our research, we automated the process of recording when a finite perturbation causes laminar flows to become turbulent in Taylor-Couette flow, the flow between two rotating, coaxial cylinders, depending on the nondimensional perturbation amplitude ($\mathcal{A}$) and Reynolds number (Re). Re is a dimensionless value describing the ratio between inertial and viscous forces and depends on the angular velocity of the rotating cylinder. As Re increases, the probability of transitioning to turbulence increases, and a smaller $\mathcal{A}$ is needed. The minimum size of the perturbation necessary to induce the transition to turbulence, known as the critical perturbation amplitude $\mathcal{A}_c$, is predicted to be related to Re by $A_c = Re^{\gamma}$. We found that $\gamma = -0.905 \pm 0.1$, which is in agreement with the upper bounds of the theoretical predictions that place γ between -4 and -1. However, it is larger than expected, and we believe this is a result of our small sample size.

Table of Contents

List of Tables

List of Figures

1 Introduction

Turbulence is the most common and preferred state for a fluid flow to exist in. It can be seen daily in examples ranging from the air moving around a car, to river currents, to smoke plumes from fires. Turbulence is marked by the unpredictable, disordered motion of fluids, coupled with eddies, vortices and random changes in velocities and pressures [BE14]. Its counterpart is the laminar flow regime, which is characterized by the basic flow of adjacent layers of fluid smoothly shearing past each other. Unlike turbulence, laminar flow has predictable flow patterns.

Along with the organic occurrence of turbulence in nature, it is also found in industrial applications due to the use of fluids in an extensive range of processes. For example, turbulent flows are very effective in mixing fluids together. This is important when pollutants are released into the environment, as exposure to a high concentration can be quite harmful to the ecosystem. Through mixing, turbulence is able to dilute and disperse pollutants in a safe manner. On the other hand, laminar flow is much more suited for basic fluid transport. Turbulence is very efficient at turning mechanical energy into heat, which means a turbulent fluid in motion converts more kinetic energy to heat than desired, and thus requires more energy to transport fluid than a laminar flow [NWB16].

Turbulence has been studied for centuries, but some of the most influential contributions have come from the scientist Osborne Reynolds, who studied turbulence in pipe flow in the late 19th century (Fig. 1.1) [Rey83]. His experiments popularized a very important value in fluid dynamics: the Reynolds number Re. This dimensionless value describes the relationship of viscous forces to inertial forces in a fluid flow. At lower Re, viscous forces dominate and the flow is laminar. At higher Re, inertia dominates and turbulence is present [BE14; NWB16].

Despite its importance, prevalence, and how long the subject has been studied, turbulence is not well understood. Especially significant is the fact that there is no general theory that can predict when a laminar flow will become turbulent [BE14]. Experimentally, engineers have been able to make some measurements on when a laminar flow should transition to turbulence based on initial conditions, but that

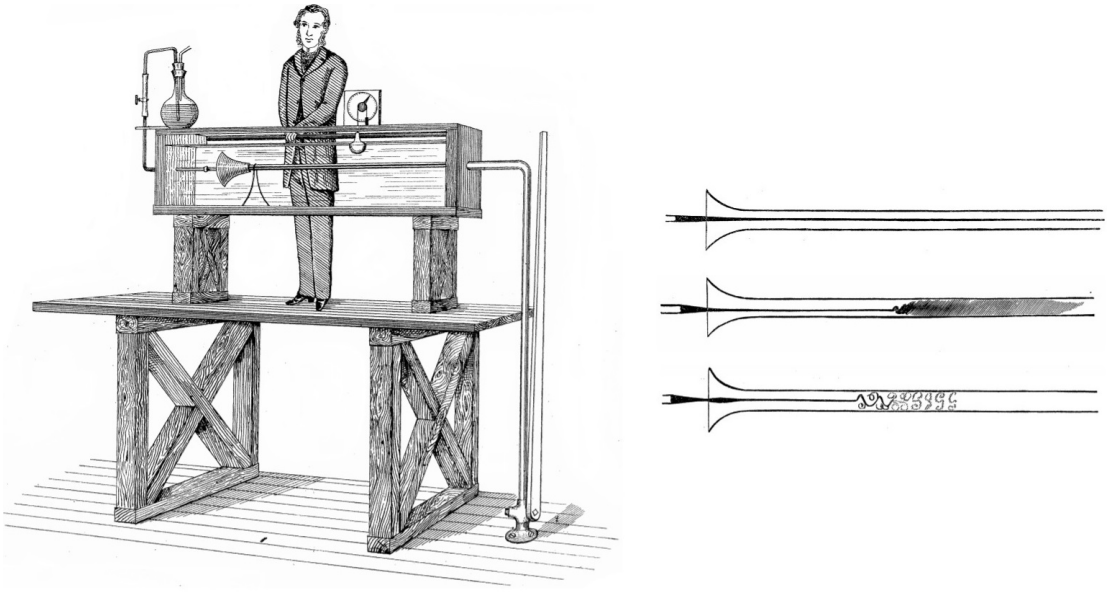

(a) (b)

Figure 1.1: (a) An illustration of Osborne Reynolds depicting him next to his apparatus for studying fluid motion in pipe flow. (b) Reynolds used dye in water to visualize the flow, as illustrated by the black markings. The top illustration shows laminar flow at low velocities, where the dye remains unmixed. The middle illustration shows laminar flow transitioning to turbulent flow, where dye begins mixing. The bottom illustration shows turbulent flow when observed by the light of electric sparks. Adapted from [Rey83].

transition point is also heavily dependent on how meticulously the experiment is constructed [AH13]. Not only that, but the underlying physical mechanisms driving turbulence is still not understood.

To better understand turbulence, we can study the relationship between different fluid flow's transition to turbulence and the Reynolds number. One flow that is unique, and the focus of this thesis, is Taylor-Couette flow, depicted in Fig. 1.2a. The Taylor-Couette system has two coaxial cylinders with different radii so as to create a gap between them where fluid is found. The radii of the inner and outer cylinders (r_i and r_o), the distance between the cylinders (d), the height of the fluid column (H), and the angular velocities of the inner and outer cylinders (ω_i and ω_o) all characterize the configuration of the Taylor-Couette system. The cylinders can rotate independently of one another, resulting in the flow regimes depicted in Fig. 1.2b. There are two different routes to transition to turbulence, either via supercritical or subcritical transition, that may occur depending on which cylinder dominates. A supercritical transition involves a gradual increase in flow complexity towards turbulence, while a subcritical transition is a sudden change from laminar to turbulent flow. The Reynolds number for each cylinder is dependent on the cylinder's angular velocity; the greater the angular velocity, the greater the Reynolds number.

Chapter 2 details more information regarding the Taylor-Couette system, the transition to turbulence, and the Reynolds number, that is necessary to understand the physics behind this thesis. Chapter 3 describes the methods utilized to set-up and execute the experimental procedure. The results of the experiment are presented in Chapter 4 and their implications are discussed in Chapter 5.

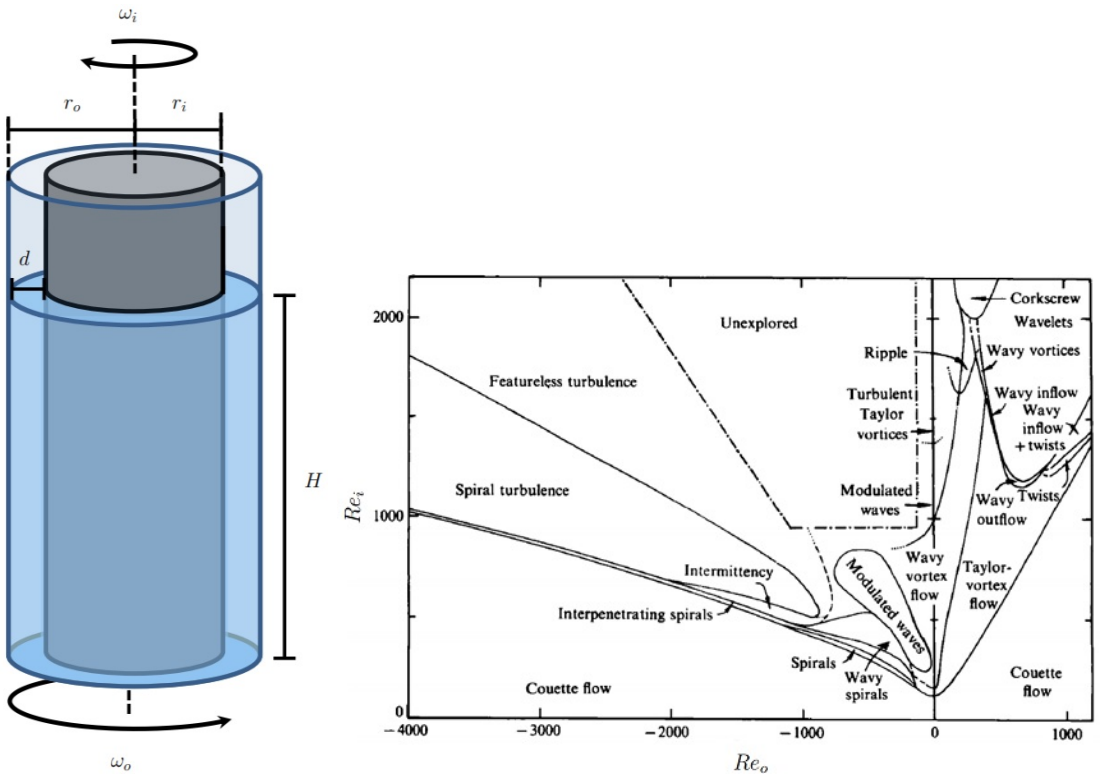

(a) (b)

Figure 1.2: (a) The Taylor-Couette apparatus has two coaxial cylinders with different radii that creates a gap between them where the fluid is found. These cylinders can rotate independently of one another, and the type of transition is dependent on which cylinder's rotation dominates. Adapted from [BE14]. (b) A variety of flow regimes are attainable depending on the combinations of angular velocities (and thus the Reynolds numbers) of the inner and outer cylinders. Re_o is the Reynolds number of the outer cylinder and Re_i is the Reynolds number of the innter cylinder. Adapted from [ALS86].

2 Background

This chapter explains the Reynolds number and transitions to turbulence in more depth, specifically with regards to the Taylor-Couette system. The explanation and importance of the critical perturbation amplitude to this research are also introduced.

2.1 Reynolds Number

Turbulent flow is defined by a high degree of spatiotemporal complexity, i.e., complexity both in space and time, and continuously irregular fluctuations in the flow velocity of the fluid [NWB16]. The transition to turbulence can be better understood in the context of the Reynolds number, where

$$Re = \frac{\text{inertial forces}}{\text{viscous forces}}.$$

When studying the inertial forces, one can consider the momenta of the different fluid elements found in the flow. For example, in a fluid with a low Reynolds number and a small flow rate, the fluid elements are traveling at a slow velocity and viscous forces have a smoothing effect that can reduce the momenta. The flow then remains laminar. On the other hand, a flow with a high Reynolds number has inertial forces dominating, thus the viscous forces are too weak to slow down the fluid elements and turbulence begins. The Reynolds number where the inertial forces overtake the viscous forces and cause a transition to turbulence is known as a critical Reynolds number, denoted as Re_c. Viscous forces depend on the viscosity of the fluid, where viscosity is a measurement of a fluid's resistance to shear. Fluids with a large viscosity, such as honey or tar, have greater viscous forces at play and therefore require greater inertial forces (in comparison to a low-viscosity fluid like water) to transition to turbulence. Assuming constant geometry, the ratio of inertial to viscous forces would still remain the same, so that flows with very different viscosities would still occur at the same Reynolds number.

In the context of Taylor-Couette system, we can easily adjust the Reynolds number in order to change the fluid regime. The kinematic viscosity, v, is determined by the fluid used, but the inertial forces can be adjusted by the angular velocity of the cylinders. A larger angular velocity results in a larger Reynolds number. We can specify the Reynolds number for both the inner cylinder, Re_i, and the outer cylinder, Re_o. The angular velocities at which they rotate are ω_i and ω_o, respectively. The two associated equations for each Reynolds number,

$$Re_i = \frac{r_i \omega_i d}{v}, \qquad Re_o = \frac{r_o \omega_o d}{v}, \tag{2.1}$$

also depend on the geometry of the system, where r_i is the radius of the inner cylinder, r_o is the radius of the outer cylinder, and d is the distance between the two cylinders, or $r_o - r_i$ [BE14]. The cylinder with the dominant angular velocity, and thus the cylinder with the dominant Reynolds number, will impact via which route a laminar Taylor-Couette flow will transition to turbulence.

2.2 Supercritical Transitions

In order to move from a laminar flow to turbulence, the flow must undergo either a supercritical transition or a subcritical transition. The supercritical transition is the more understood of the two, and is characterized by a gradual increase in spatiotemporal complexity towards turbulence. As the Reynolds number is increased, the laminar state becomes unstable, transitions to a new stable state with a more complex flow pattern, which in turn becomes unstable and transitions, and so on and so forth until turbulence is reached [BE14].

One such example is seen with convection currents, specifically Rayleigh-Bénard convection (Fig. 2.1). This flow comes about due to a temperature gradient between the top and bottom planes of a thin layer of fluid. As temperature is increased on the bottom plane, the pattern formed by convection transitions to the creation of Bénard cells on the surface. Eventually the increase in spatiotemporal complexity is great enough that the fluid flow becomes turbulent [XG95].

In the Taylor-Couette system, the supercritical transition occurs when the inner cylinder dominates. At low Reynolds number, the simple laminar flow is known as circular Couette flow, but as Re_i increases this flow bifurcates and takes on more spatial complexity in the form of Taylor vortices. Taylor vortices arise from the rotating inner cylinder pushing fluid towards the stationary outer cylinder, which then pushes the fluid back in on itself. This results in toroidal vortices of fluid that are stacked on each other. These flows are stable until, when Re_i becomes large enough, they undergo another bifurcation and become more complex until they finally transition to featureless turbulence. Figure 2.2 is an example of a supercritical transition beginning with Taylor vortex flow and eventually reaching turbulence.

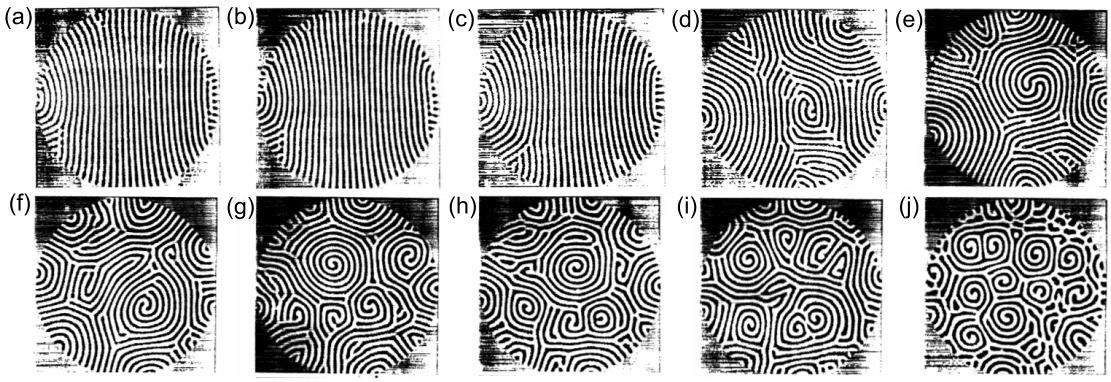

Figure 2.1: Images of Rayleigh-Bénard convection due to a temperature gradient that increases from image (a) to (j). The dark areas represent hot fluid rising, while the white areas show the cold fluid descending. Image (a) shows the global parallel roll state and by (j) the fluid flow has reached the spiral chaos state, or turbulence [XG95].

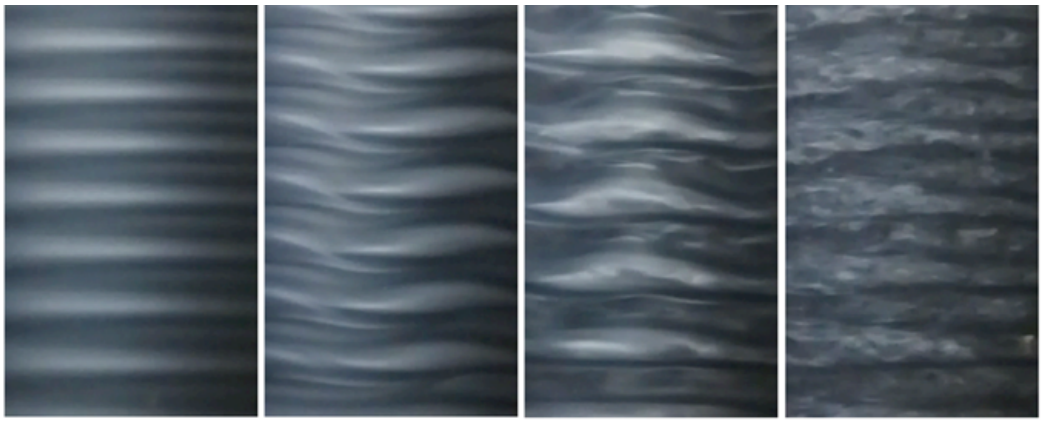

Figure 2.2: During supercritical transitions, stable flows with relatively simple spatiotemporal complexity become unstable as the angular velocity of the inner cylinder (and thus the Re_i) is increased. The Taylor vortex flow (far left) undergoes a bifurcation and transitions to wavy vortex flow, which then becomes unstable and eventually transitions into a turbulent flow (far right) [BE14].

2.3 Subcritical Transitions

The subcritical transition, on the other hand, is not marked by a gradual transition to turbulence with multiple flow patterns along the way; rather, it is characterized by a laminar flow remaining stable with an increasing Reynolds number until it suddenly becomes unstable at some Re_c and becomes turbulent. An example of a subcritical transition would be that of the pipe flow studied by Reynolds. He found that Re_c changes depending on the experimental conditions [Rey83]. This discrepancy suggests the transition is extremely sensitive to initial conditions and that turbulence must be triggered by some finite perturbation.

In the Taylor-Couette system, subcritical transition occurs when the outer cylinder rotates and the inner cylinder remains stationary. A perturbation can be introduced in a variety of ways, such as a global perturbation resulting from a short and rapid rotation of the inner cylinder, or from localized perturbations like a small obstacle or an injection of fluid. An injection of fluid into the midplane of the Taylor-Couette system will cause localized patches of turbulence, as shown in Fig. 2.3. If Re_o, the size of the perturbation, and the axial aspect ratio (the ratio of the length of the cylinder over the gap between the cylinders) are large enough, these turbulent patches can propagate into the rest of the system and cause the entire flow to become turbulent. These turbulent patches also decay; therefore, if the factors are too small, turbulence will never propagate or the lifetime of turbulence in the system will be short [BETS10; KSSH18].

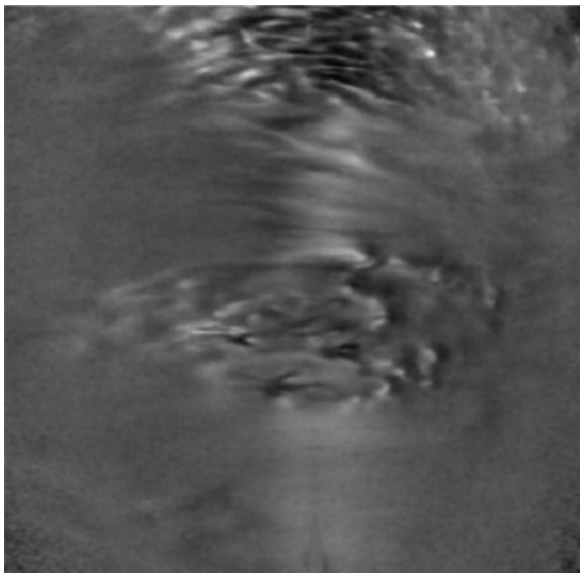

Figure 2.3: A localized turbulent patch surrounded by a laminar background [Ali11].

2.4 Scaling the Critical Perturbation Amplitude

The relationship between the amplitude of the finite perturbation and the Reynolds number help determine if a Taylor-Couette flow will transition to turbulence from that perturbation via a subcritical transition. For example, as the Reynolds number increases, the smoothing effect of viscosity is weakened, and thus a smaller finite perturbation is needed to trigger the transition [PM07]. In fact, the minimum size of the perturbation needed to trigger turbulence, known as the critical perturbation amplitude, can be scaled in relation to the Reynolds number. The critical perturbation amplitude is predicted to scale like Re^{γ}, where γ is some critical exponent between -4 and -1, depending on which physical mechanisms are included in the theoretical model [BE14; HJM03]. Borrero-Echeverry [BE14] reported a value of $\gamma = -1.9$, and Peairs, Morrison, and Borrero-Echeverry [PMBE15] found $\gamma = -1.6$. However, no consensus has been reached as to the exact value of the critical exponent. Therefore, a primary idea behind this thesis is to experimentally find which critical exponent accurately scales the critical perturbation amplitude during the subcritical transition to turbulence in Taylor-Couette flow. Finding γ will help inform the mechanisms that drive the subcritical transition.

3 Methods

This chapter will explain the apparatus and experimental methods in greater depth. It includes a description of each mechanism in the system, how the flow is visualized, how perturbations are created and characterized, how machine vision is used, and how the experiment is carried out.

3.1 Apparatus

The entire experimental design includes the Taylor-Couette system which allows for Taylor-Couette flow, the stepper motors attached to the Taylor-Couette system that rotate the cylinders, and the perturbation system that generates and injects the perturbations into the Taylor-Couette system.

3.1.1 Taylor-Couette System

The Taylor-Couette system, shown in Fig. 3.1, is comprised of two coaxial cylinders with a fluid in between. The outer cylinder has an inner radius of 5.94 cm and is made out of clear glass, thus allowing for the flow to be observed. The inner cylinder has an inner radius of 4.72 cm and is made out of aluminium that is anodized flat black [PMBE15]. This also works to help better visualize the flow. The perturbation site is the small opening on the inner cylinder connected to tubing inside the cylinder, which is then connected to the perturbation system. That small opening has a diameter of 0.11 cm.

In order to make the cylinders rotate independently, two metal bearings are placed beneath the inner and outer cylinder. O-rings are placed at the base and top of the outer cylinder to seal the system. In the gap between the two cylinders are two plastic rings, with the area between these two rings being the test section. These rings are adjustable, and the distance between the two rings determine the axial aspect ratio Γ, defined by

$$\Gamma = \frac{H}{d}, \tag{3.1}$$

and be adjusted by changing the height of the fluid column, H, and the gap between the two cylinders, d. The plastics rings are attached to the cylinders via set screws, allowing for the rings to rotate with the outer cylinder.

Figure 3.1: The Taylor-Couette apparatus is surrounded by its metal bracing. Mounted on top are the stepper motors that move the inner and outer cylinder. Through the outer cylinder, the rheoscopic fluid, white plastic rings, and black inner cylinder are visible. The tubing running to the right connects to the perturbation system, while the wire running to the left is connected to a pressure transducer. Not pictured is a USB camera which records images of the test section.

3.1.2 Perturbation System

To create the perturbations that inject into the Taylor-Couette system via the opening in the inner cylinder, we connected a Harvard Apparatus Syringe Infusion 22 syringe pump with two syringes, shown in Fig. 3.2. The syringe pump can set

different flow rates, thus we can adjust the amplitudes of the perturbations. We 3D printed parts to better stabilize the syringes as well as allow the system to both draw in and push out fluid. The syringe pump is connected to a three-way solenoid valve; depending on the position of the solenoid valve, fluid can either be pumped to a waste reservoir or to the Taylor-Couette system. This setup is illustrated in Fig. 3.3.

Figure 3.2: The Harvard Apparatus Syringe Infusion 22 syringe pump outfitted with two syringes. Via screws and the 3D printed mount, the syringes are connected to a block driven by an internal stepper motor. This block moves on a threaded rod and pushes the syringes forward or pulls them backwards to pull in or push out fluid.

The perturbation system is controlled by a Python program using an RS-232 serial interface. Initially, we set the solenoid valve to the closed position so excess fluid is pumped to the reservoir as we allow time for the syringes to build up to the specified flow rate. The solenoid valve then rapidly opens and fluid is injected into the mid-plane of the Taylor-Couette system. The solenoid valve then closes rapidly and the syringes stop pumping fluid. A Cynergy3 IPSLU-M12 pressure transducer measures the pressure in the injection line before it enters the tubing leading to the inner cylinder. The transducer is connected to a Measurement Computing USB-1208FS data acquisition device, which then transmits the data to a Python script and creates a pressure vs. time graph, which we call a pressure trace.

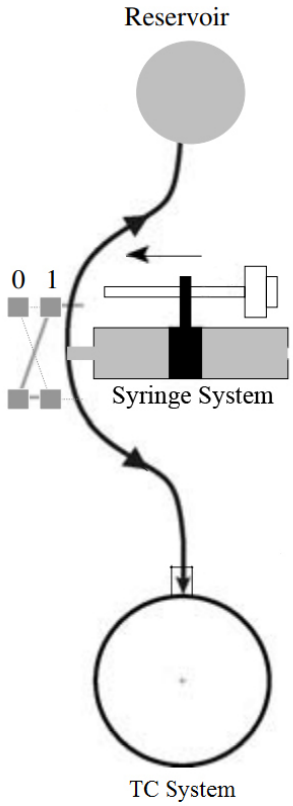

Figure 3.3: Drawing of the perturbation system with the syringe pump, reservoir, and Taylor-Couette system labeled. The solenoid valve is represented by the cross. If the valve is in position 0, then the syringe system pumps fluid to the reservoir, and if it is in position 1, then it injects a perturbation into the Taylor-Couette system [PM07].

3.2 Machine Vision

In order to decrease the labor of running the experiment by hand and increase the amount of trials, we automated the process of differentiating turbulent flow from laminar flow. We did this through the use of rheoscopic fluid, an industrial USB camera, and machine vision code written in Python.

3.2.1 Flow Visualization

To visualize the flow of the fluid, we added Barbasol shaving cream to water to create rheoscopic fluid [BECR18]. Shaving cream is used because of the stearic acid crystals in it that act as platelets that align on planes in the flow and reflect light. As the flow takes on greater spatial complexity and the stearic acid platelets

align on different planes, they reflect light differently so that the flow can be seen. Thus, when the fluid is illuminated and moving, the flow is clearly visible by reflecting light, as shown in Fig. 3.4.

3.2.2 Machine Vision Code

With the flow now visible, we utilized an IDS UI-3140CP Rev.2 monochrome camera to capture and transmit multiple grayscale images of the test section to the computer for analysis. Each grayscale image makes up a matrix, where the number of pixels that make up the image's width is the amount of columns in the matrix, and the number for the height is the amount of rows. The elements of the matrix correspond to the color of the pixel and range between 0 and 255, where 0 represents pure black and 255 represent white. We find the difference of two images by subtracting their matrices and taking the absolute value. After subtracting the first image from the second, the difference creates new pixel values, and thus we get a new image. We then set a threshold value, α, for the new image. If the difference between two pixels is equal to or greater than α, that new element in the matrix is set to `True` (which has a value of 1), and those below α are set to `False`, or 0. This process is shown in Fig. 3.4. We then sum all of the elements in the binary matrix and compare that to a second threshold, β. Then, if the new image has a sum of β or more pixels that have passed the first threshold, we conclude that there is a distinct enough difference in the images and that turbulence is present. If the new image has a sum below β, then it is deemed a laminar flow.

We programmed this image analysis to happen as new images are being taken, so the Python program knows in real time if the flow is turbulent or not. We set the camera to initially wait a certain amount of time until turbulence is detected. If that never happens, then the perturbation and angular velocity were not great enough to produce turbulence, and the flow is deemed laminar. If it is detected, then the camera continues collecting images until a set time after turbulence is undetected. We set the wait time in case the flow appears to briefly relaminarize before becoming turbulent once again. The program also records the duration of turbulent flow.

3.2.3 Defining the Camera Thresholds

In order to define the first camera threshold, we applied the technique used by Alidai to maximize the amount of turbulent pixels in turbulent flow and minimize the amount in laminar flow [Ali11]. We defined the signal to noise ratio, f, as

$$f(\alpha) = \frac{(100 - R_L) + R_T}{(100 - R_T) + R_L}, \tag{3.2}$$

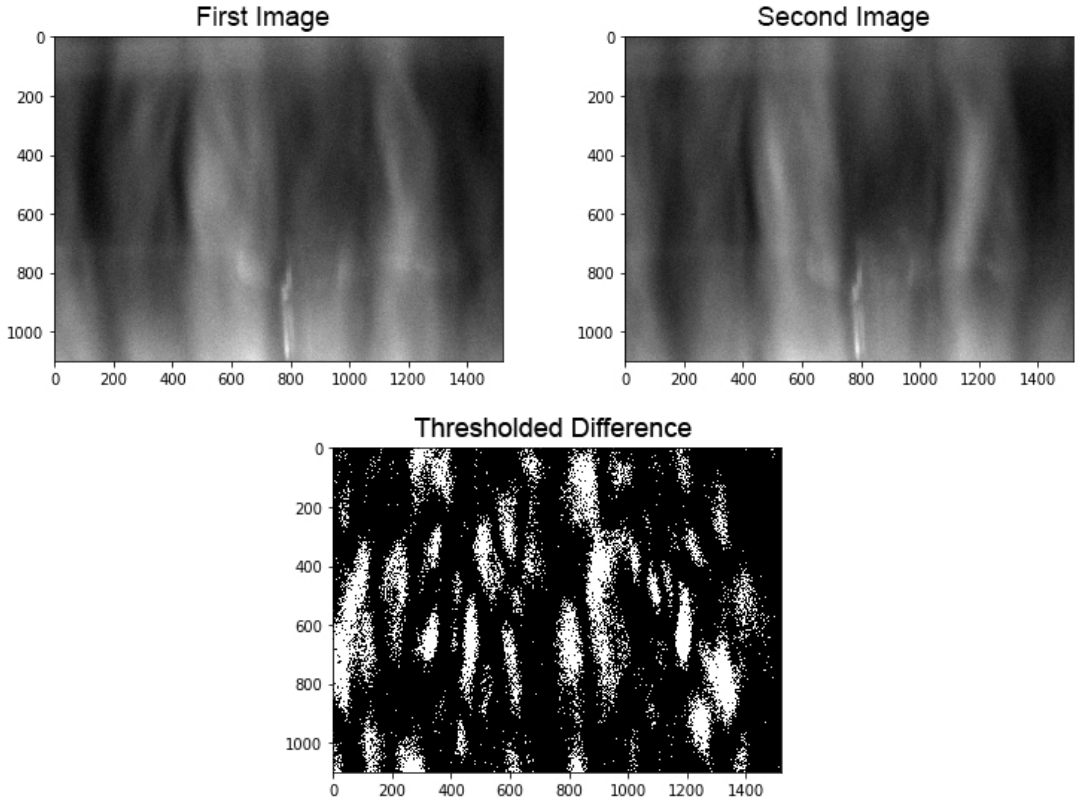

Figure 3.4: The first image and second image are taken a quarter of a second apart and then compared to α. The number of pixels are on the horizontal and vertical axes. All white pixels in the bottom image represent turbulent pixels, while the black ones are laminar pixels.

where α is the threshold value, R_L is the percentage of turbulent pixels in laminar flow, and R_T is the percentage of the turbulent pixels in turbulent flow. We took 100 images for each α tested and found the average value of $f(\alpha)$ for those 100 images (Fig. 3.5). The maximum value, which represents the best possible threshold, was $\alpha = 8$.

To define the second threshold value, β, we kept the flow laminar and manually tested the machine vision code with different values. We approximately determined the lowest value that always recognized the flow as laminar, and then increased that value by about 15%. We found that $\beta = 78000$ was around the lowest value, and thus increased it to $\beta = 90000$ as our final threshold.

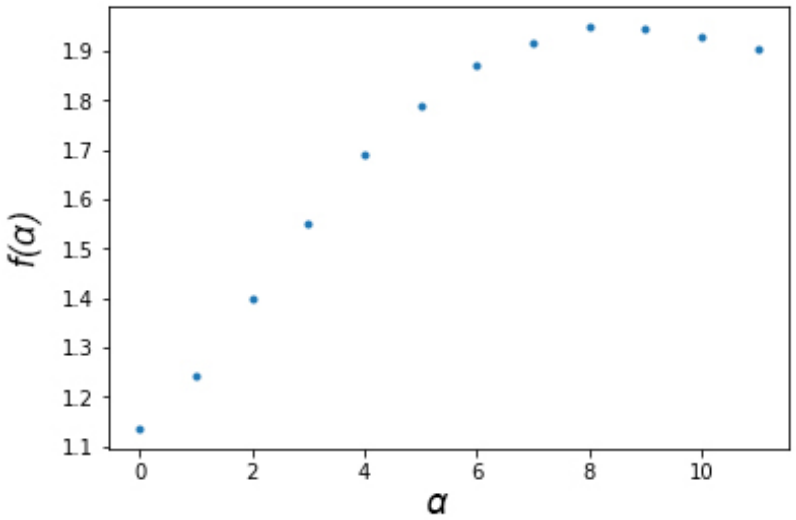

Figure 3.5: The signal to noise ratio function $f(\alpha)$ versus the first threshold value α.

3.3 Experimental Methods

The Taylor-Couette system, perturbation system, and machine vision code are all automated in the same Python script and allow for many trials of data to be taken. By using the `threading` module, multiple processes can be run simultaneously.

3.3.1 Characterizing the Perturbations

In order for data to be comparable across trials, the perturbations need to have similarly shaped pressure traces. The optimal shape for this is a "boxcar" shape, shown in Fig. 3.6b. The boxcar shape has a sharp increase of pressure into the midplane of the Taylor-Couette system when the solenoid valve opens, an even amount of pressure, and then a sharp drop off once the valve closes. This way, we are able to independently change the amplitude or duration of the perturbations but still have a comparable shape [PM07].

Initially, we only saw the sharp drop-off in pressure at the end of the perturbation's pressure trace, as shown in Fig. 3.6a. We approached achieving this boxcar shape and ensuring the perturbations are reproducible in multiple ways. The first action was to use a wider bin for the reservoir, therefore water level rose at a much slower rate as we discarded excess fluid. This is important since the greater the water level in the reservoir, the more pressure builds up before the solenoid valve opened. By changing this, we ensured that trials early on would not have vastly different initial pressures than later trials. In order to recreate the sharp beginning of the trace, we built up pressure by attaching an adjustable needle valve to

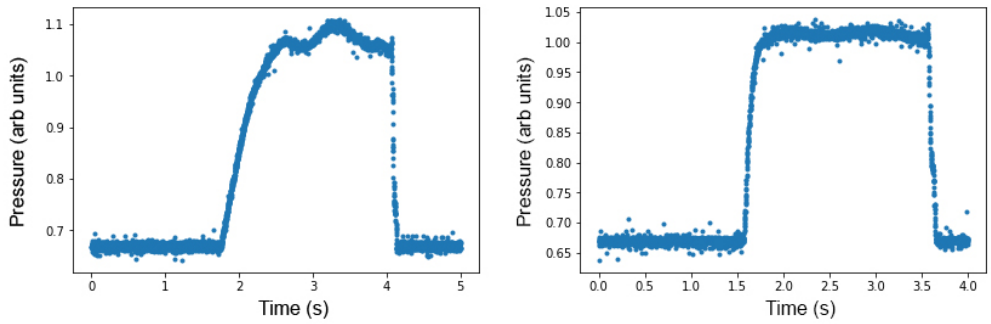

(a) (b)

Figure 3.6: (a) The typical shape of the pressure traces we initially saw during our research. (b) Pressure trace of a perturbation illustrating the necessary boxcar shape. We achieved this shape after modifications to our system.

the end of the tubing leading to the the reservoir. Thus, when the solenoid valve opens, the pressure going to the Taylor-Couette apparatus increases greatly and rapidly. Finally, to ensure that the injection is at an even flow rate, we tightened a gear belt on the syringe pump system and 3D printed sturdier plastic mounts for the syringes. This made sure the syringes moved consistently each time.

3.3.2 Conducting the Experiment

To conduct the experiment, all air needs to be removed from the tubing and syringes so as not to create unwanted perturbations. When that is achieved, the needle valve must be closed enough to create sufficient initial pressure but not enough to stall the motor driving the syringe pump. The stepper motor controlling the inner cylinder system is engaged and keeps the inner cylinder in place, while the stepper motor for the outer cylinder accelerates the flow to the desired Re_o specified in the Python program. The flow is allowed to keep running for one minute to ensure the flow is laminar and has reached the desired Reynolds number. Next, the camera begins recording while the perturbation system starts and injects a perturbation at a specified flow rate. If the perturbation amplitude is too small to trigger turbulence, then the camera stops recording and records the trial as not triggering turbulence. If the flow does transition to turbulence, then the camera will keep recording until it relaminarizes or 30 seconds pass. This combination of Re_o and perturbation amplitude is then recorded as having triggered turbulence. The pump is run in reverse to return the amount of water in the Taylor-Couette system and the syringes to the original amount at the start of the trial. This code then repeats for ten trials before a new trial is started for a different Reynolds number or perturbation amplitude.

4 Data and Discussion

This chapter will present the data collected and then discuss the shortcomings and implications of that data. While the data set is not large enough to conclusively state a value for γ, the results and means of analysis still merit inclusion.

4.1 Data

Using the experimental procedure outlined in Chapter 3, we tested the probability of transitioning to turbulence with various combinations of Q_{jet}, the perturbation's volume flow rates, and Re_o, the outer Reynolds number. Each perturbation lasted five seconds, and had flow rates ranging from 0.433 mL/s to 0.833 mL/s, with data taken in 0.033 mL/s intervals. The Reynolds number ranged from 12320 to 16668, with data taken in 725 intervals. For every combination, we ran ten trials and then found the proportion of those trials that transitioned to turbulence. The results are shown in Table 4.1. The data points are color-coded, where dark green boxes represent combinations where all all ten trials transitioned to turbulence, red boxes represent all ten trials remaining laminar, and the color gradient between red and green represent the proportions between 0 and 1. The missing data is represented by the white boxes in the table.

4.2 Critical Perturbation Amplitude

In order to find the critical exponent γ that scales the critical perturbation amplitude, we first converted the perturbation amplitudes into nondimensional values with the formula used by Peixinho and Mullin [PM07]. This nondimensional perturbation amplitude, known as $\mathcal{A}$, also allows for comparison between experiments with different systems and geometries. $\mathcal{A}$ is made nondimensional by scaling the

Q_{jet} (mL/s) \ $\mathbf{Re}_o$	12320	13044	13769	14494	15218	15943	16668
0.833	0.00	0.00	0.10	0.50	1.00	1.00	1.00
0.800	0.00	0.30	0.40	0.70	1.00	1.00	1.00
0.767	0.00	0.10	0.30	0.70	1.00	1.00	1.00
0.733	0.00	0.10	0.40	0.70	0.90	1.00	1.00
0.700	0.10	0.00	0.20	0.70	0.80	1.00	
0.667	0.20	0.70	0.70	1.00	0.90	1.00	
0.633	0.30	0.20	0.60	0.80	1.00	1.00	1.00
0.600	0.20	0.70	0.90	0.80	1.00		
0.567	0.10	0.50	1.00	0.90	0.90		
0.533	0.20	0.90	1.00	0.80	1.00		
0.500	0.00	0.10	0.70	1.00	1.00		
0.467	0.00	0.00	0.00	0.60	0.90		
0.433	0.00	0.00	0.00	0.00	0.40		

Table 4.1: The proportion of a five second perturbation transitioning to turbulence with different flow rates and outer Reynolds number, with each data point representing the proportion of ten trials in which turbulence was induced. The green boxes correspond to greater probability of transitioning, while the red boxes correspond to a smaller probability. The white boxes represent data that was not taken.

flux through the injection site by the flux through the meridional plane of the Taylor-Couette system [BE14]. Thus, $\mathcal{A}$ is given by:

$$\mathcal{A} = \frac{\Phi_{jet}}{\Phi_{TC}} = \frac{Q_{jet}}{\pi r_{jet}^2 U_o}, \tag{4.1}$$

where r_{jet} is the radius of the injection site, and U_o is the speed of the outer wall, that is, $r_o\omega_o$.

Since we evaluate γ for the scaling of the critical perturbation amplitude, $\mathcal{A}_c$ is analysed. $\mathcal{A}_c$ must be assigned to a point where a set proportion of trials always transitions to turbulence. For our research, we used 0.85. We then linearly interpolated the data for each Re_o to find the estimated $\mathcal{A}_c$. As the range of our data was limited, we only used $Re_o = 13044, 13769, 14494$, and 15218. We then graphed the log-log plot of the four points and found the slope of the best-fit line from least-square regressions. The results are plotted in Fig. 4.1. This slope, and therefore γ, was equal to -0.905 ± 0.1.

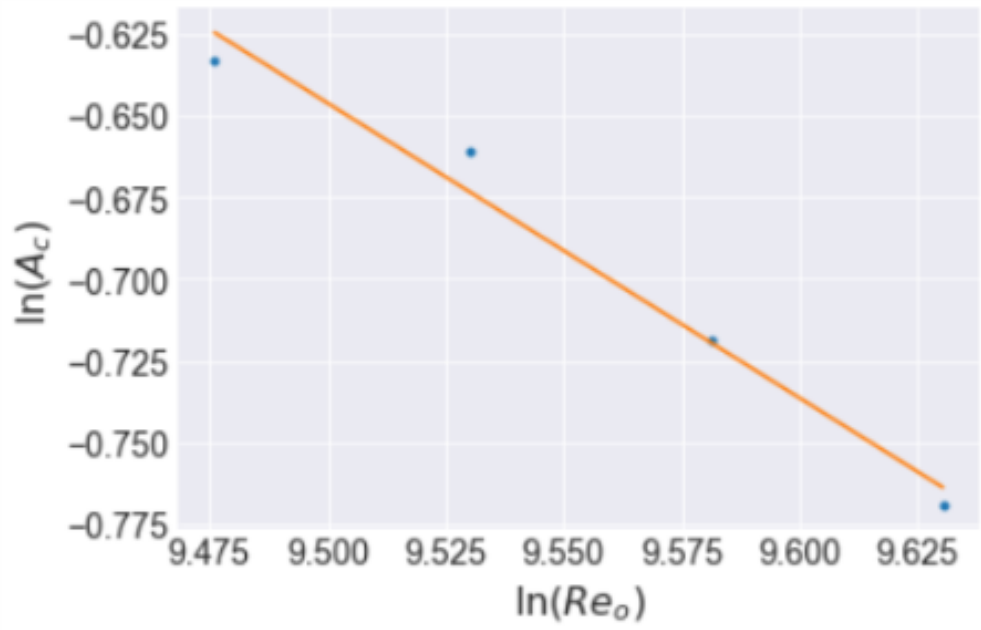

Figure 4.1: The blue dots are points where 0.85 of trials transitioned to turbulence for various combinations of $\ln(\mathcal{A}_c)$ and $\ln(Re_o)$, and the orange line is the best-fit line of these points using least-squares regression. The slope of the best-fit line is $\gamma = -0.905 \pm 0.1$.

4.3 Discussion

There are some immediate problems to note with our data. Firstly, we only collected ten trials per data point, which is significantly less than what is needed to confidently calculate γ or to reduce the statistical uncertainty inherent in the transition to turbulence. At best, it can experimentally give us a rough outline of the relationship between Re_o and Q_{jet}, as well as generally explain what combinations should lead to a laminar flow always remaining laminar or always transitioning to turbulence. Secondly, not only did the data set use too few of trials, but the range of data collected was very limited and missing important values. Due to the short period of time that the Taylor-Couette apparatus was operational, only this data could be taken.

From the results that we did have, we saw the proportion of trials transitioning to turbulence increasing with an increasing Re_o. This was expected from theory and past experiments. As the outer Reynolds number grows, inertial forces become more dominant. Viscous forces cannot "smooth" the momenta of the fluid elements, which allows turbulent patches to propagate more easily. In regards to the effect of the perturbation amplitude on the proportion of trials transitioning, however, we did not see the expected results. What we expected is that a flow with a greater Reynolds number requires a smaller perturbation to induce turbulence, but instead, the third problem to note in our data was that an increasing Q_{jet}, and thus an increasing $\mathcal{A}_c$, did not always increase the proportion of trials transitioning. This was especially apparent in the Table 4.1 column when $Re_o = 13044$: when $Q_{jet} = 0.533$ mL/s, there was a proportion of trials transitioning of 0.9, whereas the larger $Q_{jet} = 0.833$ mL/s data point had a proportion of 0. These unexpected results were most likely due to the small sample size, as it did not allow for enough data to model the true proportion.

Finally, our calculations of $\mathcal{A}$, and therefore $\mathcal{A}_c$ and γ, were larger than expected. Despite using the same apparatus, Peairs, Morrison, and Borrero-Echeverry [PMBE15] had $\mathcal{A}$ values ranging from 0.01 to 0.04, whereas we calculated $\mathcal{A}$ values from 0.35 to 0.92. Having $\mathcal{A}_c$ be larger by an order of a magnitude results in $\gamma = -0.905 \pm 0.1$ which is in the upper bound of theoretically predicated range of [-4, -1] supported by previous research. Furthermore, since the data collected did not have the steady increase or decrease in proportion of trials transitioning when Q_{jet} was varied, the data points we interpolated between may not have been the correct points.

5 Conclusion

This goal of this research was to find the relationship between the critical perturbation amplitude, which is the minimum size of a perturbation needed to induce a subcritical transition to turbulence in Taylor-Couette flow, and the outer Reynolds number of the flow. Specifically, we were interested in finding the value of the critical exponent γ that scales the critical perturbation amplitude by the outer Reynolds numberto the power of γ, that is, $\mathcal{A}_c = Re_o^{\gamma}$. The value that we calculated was $\gamma = -0.905 \pm 0.1$, which is in agreement with the predicted range of -4 to -1, though larger than we expected. We believe that this may not be the true value, but rather is a result of the small data set and complications in converting to the nondimensional perturbation amplitude. Borrero-Echeverry [BE14] reported a value of $\gamma = -1.9$, and Peairs, Morrison, and Borrero-Echeverry [PMBE15] found $\gamma = -1.6$. The latter study is especially important when comparing results, as the apparatus and geometry of the system is the exact same as that of our work.

Despite the shortcomings of our data set and calculation of γ, the research was successful in automating the process of data collection of large trials. Therefore, we highly suggest that researchers continuing this study should expand the range of data collected as well as increase the number of trials per data point from ten trials to 100 trials. Future research should also work on improving the shape of the perturbation amplitude, as it inconsistently followed the "boxcar" pressure trace function during data collection. Finally, considering that the transition to turbulence is so heavily sensitive to initial conditions, we suggest adding a temperature control to the system, in order to reduce outside factors and ensure that trials are more comparable.

Bibliography

[AH13] K. Avila and B. Hof, *High-precision Taylor-Couette experiment to study subcritical transitions and the role of boundary conditions and size effects*, Review of Scientific Instruments **84** (2013), no. 6, 065106.

[Ali11] A. Alidai, *Transient Turbulence in Taylor Couette Flow*, Master's thesis, Delft University of Technology, 2011.

[ALS86] C. David Andereck, S. S. Liu, and Harry L. Swinney, *Flow Regimes in a Circular Couette System with Independently Rotating Cylinders*, Journal of Fluid Mechanics **164** (1986), 155.

[BE14] D. Borrero-Echeverry, *Subcritical Transition to Turbulence in Taylor-Couette Flow*, Ph.D. thesis, Georgia Institute of Technology, 2014.

[BECR18] D. Borrero-Echeverry, C. J. Crowley, and T. P. Riddick, *Rheoscopic Fluids in a Post-Kalliroscope World*, Physics of Fluids **30** (2018), no. 8, 087103.

[BETS10] D. Borrero-Echeverry, R. Tagg, and M. F. Schatz, *Transient Turbulence in Taylor-Couette Flow*, Physical Review E **81** (2010), no. 2.

[HJM03] B. Hof, A. Juel, and T. Mullin, *Scaling of the Turbulence Transition Threshold in a Pipe*, Physical Review Letters **91** (2003), no. 24, 244502/4.

[KSSH18] J. Kühnen, D. Scarselli, M. Schaner, and B. Hof, *Relaminarization by Steady Modification of the Streamwise Velocity Profile in a Pipe*, Flow, Turbulence and Combustion **100** (2018), 919–943.

[NWB16] F. T. M. Nieuwstadt, J. Westerweel, and B. J. Boersma, *Turbulence: Introduction to Theory and Applications of Turbulent Flows*, (Springer International Publishing, Switzerland, 2016).

[PM07] J. Peixinho and T. Mullin, *Finite-Amplitude Thresholds for Transition in Pipe Flow*, Journal of Fluid Mechanics **582** (2007), 169.

[PMBE15] E. Peairs, B. C. Morrison, and D. Borrero-Echeverry, *Finite-Amplitude Thresholds in Taylor-Couette Flow*, Unpublished (2015).

[Rey83] O. Reynolds, *An Experimental Investigation of the Circumstances Which Determine Whether the Motion of Water Shall Be Direct or Sinuous, and of the Law of Resistance in Parallel Channels*, Philosophical Transactions of the Royal Society of London **174** (1883), 935–982.

[XG95] H. Xi and J. D. Gunton, *Spatiotemporal Chaos in a Model of Rayleigh-Bénard Convection*, Physical Review E **52** (1995), 4963–4975.